Nanosecond sum-frequency generating optical parametric oscillator using simultaneous phase matching

Z. Gürkan Figen and Orhan Aytür

Department of Electrical and Electronics Engineering,
Bilkent University, Ankara, Turkey

aytur@ee.bilkent.edu.tr

Abstract: We report a nanosecond sum-frequency generating optical parametric oscillator based on a single $KTiOAsO_4$ crystal that is simultaneously phase matched for optical parametric generation and sum-frequency generation. Pumped at a wavelength of 1064 nm by a *Q*-switched Nd:YAG laser, this device produces 10.4-ns-long 8.3 mJ red pulses at a wavelength of 627 nm with 21% energy conversion efficiency. This device provides a simple and efficient method for converting high energy Nd:YAG lasers to a red wavelength.

© 2005 Optical Society of America

OCIS codes: (190.2620) Frequency conversion; (190.4970) Parametric oscillators and amplifiers; (190.4360) Nonlinear optics, devices; (190.7220) Upconversion; (140.3530) Lasers, neodymium; (140.3540) Lasers, Q-switched.

References and links

1. W. R. Bosenberg, L. K. Cheng, and C. L. Tang, "Ultraviolet optical parametric oscillation in β-BaB_2O_4," Appl. Phys. Lett. **54,** 13–15 (1989).
2. A. Fix, T. Schröder, and R. Wallenstein, "The optical parametric oscillators of beta-barium borate and lithium triborate: new sources of powerful tunable laser radiation in the ultraviolet, visible and near infrared," Laser Optoelektron. **23,** 106–110 (1991).
3. D. E. Withers, G. Robertson, A. J. Henderson, Y. Tang, Y. Cui, W. Sibbett, B. D. Sinclair, and M. H. Dunn, "Comparison of lithium triborate and β-barium borate as nonlinear media for optical parametric oscillators," J. Opt. Soc. Am. B **10,** 1737–1743 (1993).
4. A. Fix, T. Schröder, R. Wallenstein, J. G. Haub, M. J. Johnson, and B. J. Orr, "Tunable β-barium borate optical parametric oscillator: operating characteristics with and without injection seeding," J. Opt. Soc. Am. B **10,** 1744–1750 (1993).
5. U. Bäder, J.-P. Meyn, J. Bartschke, T. Weber, A. Borsutzky, R. Wallenstein, R. G. Batchko, M. M. Fejer, and R. L. Byer, "Nanosecond periodically poled lithium niobate optical parametric generator pumped at 532 nm by a single-frequency passively *Q*-switched Nd:YAG laser," Opt. Lett. **24,** 1608–1610 (1999).
6. V. Pasiskevicius, H. Karlsson, F. Laurell, R. Butkus, V. Smilgevicius, and A. Piskarskas, "High-efficiency parametric oscillation and spectral control in the red spectral region with periodically poled KTiOPO," Opt. Lett. **26,** 710–712 (2001).
7. R. A. Andrews, H. Rabin, and C. L. Tang, "Coupled parametric downconversion and upconversion with simultaneous phase matching," Phys. Rev. Lett. **25,** 605–608 (1970).
8. S. N. Zhu, Y. Y. Zhu, and N. B. Ming, "Quasi-phase-matched third-harmonic generation in a quasi-periodic optical superlattice," Science **278,** 843–846 (1997).
9. O. Pfister, J. S. Wells, L. Hollberg, L. Zink, D. A. Van Baak, M. D. Levenson, and W. R. Bosenberg, "Continuous-wave frequency tripling and quadrupling by simultaneous three-wave mixings in periodically poled crystals: application to a two-step 1.19–10.71-μm frequency bridge," Opt. Lett. **22,** 1211–1213 (1997).
10. K. G. Köprülü, T. Kartaloğlu, Y. Dikmelik, and O. Aytür, "Single-crystal sum-frequency-generating optical parametric oscillator," J. Opt. Soc. Am. B **16,** 1546–1552 (1999).
11. X. P. Zhang, J. Hebling, J. Kuhl, W. W. Rühle, and H. Giessen, "Efficient intracavity generation of visible pulses in a femtosecond near-infrared optical parametric oscillator," Opt. Lett. **26,** 2005–2007 (2001).

12. K. Fradkin-Kashi, A. Arie, P. Urenski, and G. Rosenman, "Multiple nonlinear optical interactions with arbitrary wave vector differences," Phys. Rev. Lett. **88,** 023903 (2002).

13. T. Kartaloğlu, Z. G. Figen, and O. Aytür, "Simultaneous phase matching of optical parametric oscillation and second-harmonic generation in aperiodically poled lithium niobate," J. Opt. Soc. Am. B **20,** 343–350 (2003).

14. T. Kartaloğlu and O. Aytür, "Femtosecond self-doubling optical parametric oscillator based on KTiOAsO$_4$," IEEE J. Quantum Electron. **39,** 65–67 (2003).

15. T. W. Ren, J. L. He, C. Zhang, S. N. Zhu, Y. Y. Zhu, and Y. Hang, "Simultaneous generation of three primary colours using aperiodically poled LiTaO$_3$," J. Phys. Condens. Matter **16,** 3289–3294 (2004).

16. Y. Dikmelik, G. Akgün, and O. Aytür, "Plane-wave dynamics of optical parametric oscillation with simultaneous sum-frequency generation," IEEE J. Quantum Electron. **35,** 897–912 (1999).

17. D. L. Fenimore, K. L. Schepler, U. B. Ramabadran, and S. R. McPherson, "Infrared corrected Sellmeier coefficients for potassium titanyl arsenate," J. Opt. Soc. Am. B **12,** 794–796 (1995).

18. J.-P. Fève, B. Boulanger, O. Pacaud, I. Rousseau, B. Ménaert, G. Marnier, P. Villeval, C. Bonnin, G. M. Loiacono, and D. N. Loiacono, "Phase-matching measurements and Sellmeier equations over the complete transparency range of KTiOAsO$_4$, RbTiOAsO$_4$, and CsTiOAsO$_4$," J. Opt. Soc. Am. B **17,** 775–780 (2000).

19. K. Kato, N. Umemura, and E. Tanaka, "90° phase-matched mid-infrared parametric oscillation in undoped KTiOAsO$_4$," Jpn. J. Appl. Phys. **36,** L403–L405 (1997).

1. Introduction

Laser sources in the red part of the spectrum have several important applications in areas such as display technologies, holography, biomedical systems, materials processing, and basic science. Efficient conversion of well-established lasers such as the Nd:YAG laser to red wavelengths is an attractive approach to red generation, especially beyond power or energy levels that are attainable with semiconductor lasers. Second, third, and fourth harmonic generation of Nd:YAG lasers are commonly used to make green or UV sources. However, conversion to red wavelengths usually requires cascading harmonic generation with optical parametric generation. Generation of red laser beams using optical parametric oscillators (OPOs) that are pumped by various harmonics of the Nd:YAG laser were previously reported in the nanosecond pulsed regime [1–4]; however, the overall 1064-nm-to-visible energy conversion efficiencies of these systems are typically below 10%. A nanosecond periodically poled lithium niobate (PPLN) OPO pumped by the second-harmonic of a Q-switched Nd:YAG laser was reported to achieve a maximum of 12% conversion efficiency [5]; however, the output energy was limited due to the damage threshold of the lithium niobate crystal that is imposed by aperture limitations. Similarly, a recently reported nanosecond periodically-poled potassium titanyl phosphate (PP-KTP) OPO that is pumped at 532 nm [6] also suffers from output energy limitations imposed by the damage threshold, a general problem resulting from aperture-size constraints in crystal poling.

An alternative to cascading two steps of nonlinear frequency conversion is to combine them within the same nonlinear crystal using simultaneous phase matching. This technique has been demonstrated to provide efficient frequency conversion to wavelengths that cannot be reached via a single nonlinear process [7–15]. In particular, both femtosecond and continuous-wave Ti:sapphire laser beams were upconverted to visible wavelengths by combining sum-frequency generation (SFG) [10, 11] or second-harmonic generation [11, 13, 14] with optical parametric oscillation.

In this paper, we report a nanosecond sum-frequency generating OPO (SF-OPO) in which a single KTiOAsO$_4$ (KTA) crystal is used for both parametric generation and SFG. Pumped by a nanosecond Q-switched Nd:YAG laser at 1064 nm, this compact device generates red output pulses at 627 nm with more than 20% 1064-nm-to-627-nm energy conversion efficiency. To our knowledge, this is the first demonstration of simultaneous phase matching within an optical parametric oscillator operating in the nanosecond regime.

2. Experimental configuration

Our KTA crystal was designed so that when pumped at 1064 nm, it is simultaneously phase matched for optical parametric generation and SFG at the signal and pump wavelengths. Type-II birefringent phase matching facilitates optical parametric generation of a *p*-polarized (horizontal, fast axis) signal beam at 1525 nm and an *s*-polarized (vertical, slow axis) idler beam at 3520 nm from the *p*-polarized pump beam at 1064 nm. SFG with an *s*-polarized beam at the signal wavelength and a *p*-polarized beam at the pump wavelength as its inputs is simultaneously phase-matched for the same direction of propagation in the KTA crystal, again in a type-II polarization geometry. Coupling a portion of the *p*-polarized intracavity signal beam to *s*-polarization with a retarder plate facilitates the generation of a *p*-polarized sum-frequency output beam at 627 nm. This simultaneous phase matching polarization geometry belongs to class-D SF-OPOs, as defined in Ref. [16].

Our SF-OPO is based on a 20-mm-long KTA crystal that is cut along the $\theta = 90°$ and $\phi = 33°$ direction. It has antireflection coatings for the signal and pump wavelengths on both surfaces. However, experimentally we determined that simultaneous phase matching at our wavelengths occurs at $\theta = 90°$ and $\phi = 30.1°$, requiring a corresponding tilt. This propagation angle is very close to the value calculated using the Sellmeier coefficients given in Ref. [17] for parametric generation and those given in Ref. [18] for SFG. While the beams polarized along the slow axis (*z*-axis) experience no walk-off, the calculated walk-off angles associated with the beams polarized along the fast axis are relatively small, with the maximum value being $0.15°$ for the sum-frequency beam.

Our experimental setup is shown in Fig. 1. The pump source is a 4 Hz flash-lamp-pumped *Q*-switched Nd:YAG laser operating at 1064 nm, generating 40 mJ pulses of 14.7 ns duration (FWHM). The telescope lenses reduce the diameter of the pump beam that has a Gaussian-like spatial profile almost 2.5-fold resulting in a 1.6-mm-diameter beam ($1/e^2$ intensity point) with a divergence of 0.8 mrad. We calculated the peak pump intensity at the crystal to be 260 MW/cm^2 under these circumstances. We chose not to increase our pump intensity any further than this, since the damage threshold of the surface coatings on the KTA crystal are specified to be 500 MW/cm^2 for a 20-ns pulse at 1064 nm.
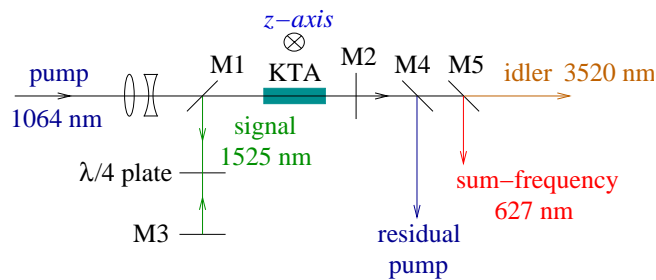
Fig. 1. Experimental setup of the SF-OPO.

The 4.8-cm-long L-shaped cavity is made up of three flat mirrors, M1, M2, and M3, which are all high reflectors at the signal wavelength. The pump beam enters the cavity through M1 and exits the cavity through M2, making a single pass. Both these mirrors are also high transmitters at 1064 nm. When pumped above threshold, a *p*-polarized intracavity signal beam is generated. An intracavity $\lambda/4$ plate whose surfaces are antireflection coated at 1525 nm acts as a polarization rotator to couple a portion of the signal beam to *s*-polarization. Simultaneously phase-matched SFG results in the *s*-polarized component of the signal to be summed with the pump beam to produce a sum-frequency beam at 627 nm. This red beam exits the cavity through

M2. The residual pump and red output beams are separated from each other using dichroic mirrors M4 and M5. The idler beam at 3520 nm is mostly absorbed in M2, M4, and M5, which are made from BK7 glass. Only a small amount of idler, 0.4 mJ at the highest input pulse energy, is measured after these mirrors.

3.   Results and discussion

In the SF-OPO, there is an optimum polarization rotation angle that maximizes the output pulse energy. When the fast axis of the intracavity retarder plate is aligned with either the *p*- or *s*-polarization direction, there is no polarization rotation. In this case, the intracavity signal beam does not have an *s*-polarized component and hence there is no SFG. The residual cavity losses experienced by the signal beam is relatively small (approximately 3%), resulting in a low OPO threshold and high intracavity signal intensity. As the polarization rotation angle is increased by rotating the retarder plate, a portion of the *p*-polarized intracavity signal is coupled into *s*-polarization and SFG begins to take place. However, rotating the signal polarization effectively increases the total linear cavity loss experienced by the resonating *p*-polarized signal, increasing the OPO threshold. Consequently, at some polarization rotation angle above the optimum value, SF-OPO falls below threshold.
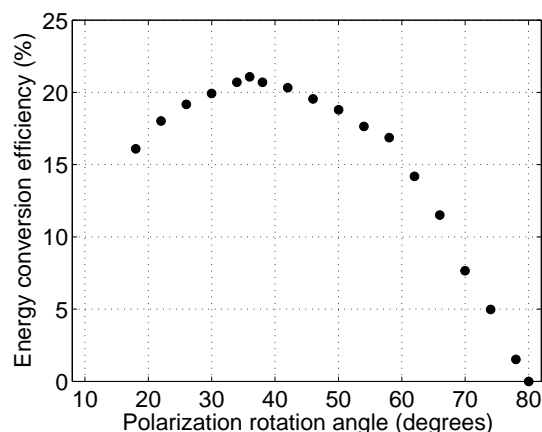
Fig. 2. Sum-frequency energy conversion efficiency as a function of the polarization rotation angle. Pump energy is held fixed at 39.2 mJ.

Figure 2 shows the 1064-nm-to-627-nm energy conversion conversion efficiency as a function of the polarization rotation angle at a fixed pump energy of 39.2 mJ. The smallest polarization rotation angle is chosen to be $18°$ to avoid damage to the KTA crystal. A peak conversion efficiency of 21% is obtained at an optimum polarization rotation angle of $36°$. The SF-OPO falls below threshold at $80°$.

Figure 3 shows the output sum-frequency energy and pump depletion as functions of the pump energy while the polarization rotation angle is held fixed at $36°$. A maximum of 8.3 mJ sum-frequency energy is obtained at a pump energy of 39.5 mJ, corresponding to 21% conversion efficiency and 37% pump depletion. The threshold energy of the SF-OPO is 16.7 mJ at this rotation angle.

For any input pump level, the output sum-frequency energy can easily be maximized by adjusting the polarization rotation angle. Figure 4 shows the maximum energy conversion efficiency and the optimum polarization rotation angle as functions of the input pump energy.
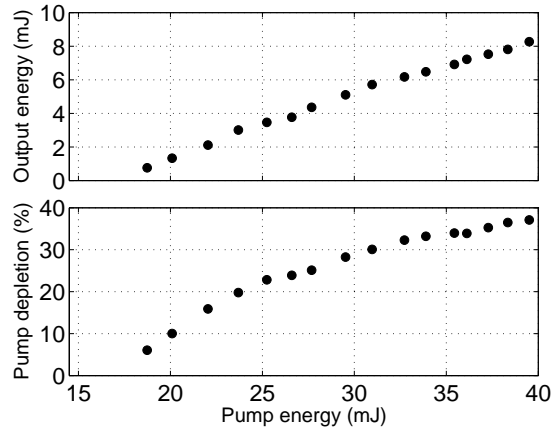
Fig. 3. Output sum-frequency energy and pump depletion as functions of pump energy. Polarization rotation angle is held fixed at 36°.
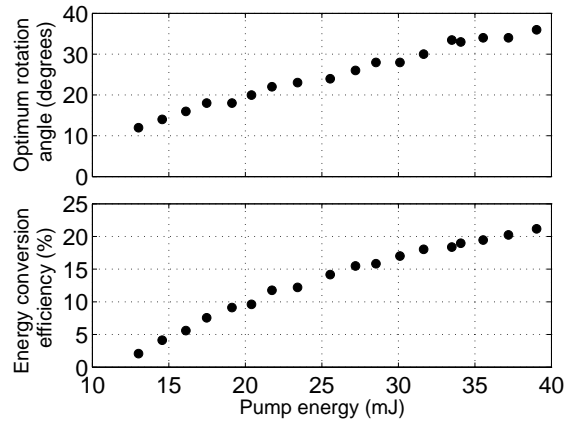
Fig. 4. Optimum polarization rotation angle and maximum energy conversion efficiency as functions of pump energy.

The spectrum of the sum-frequency output obtained at full energy is shown in Fig. 5. The bandwidths of the pump and sum-frequency spectra are approximately 0.2 nm. The pulse durations (FWHM) of the sum-frequency, intracavity signal and pump beams are 10.4 ns, 13.2 ns and 14.7 ns, respectively.

The simultaneous phase-matching angle of parametric generation and SFG was experimentally determined to be $\theta = 90°$ and $\phi = 30.1°$. Figure 6 shows the sum-frequency energy at a fixed polarization rotation angle of $28°$ and signal energy at a polarization rotation angle of $0°$ (no SFG) as functions of the internal propagation angle ϕ ($\theta = 90°$). An output coupler with a reflectivity of $R = 85\%$ at the signal wavelength was used for this measurement. The input pump energy was fixed at 40 ± 0.6 mJ and the pump beam had a diameter of 2.2 mm ($1/e^2$ intensity point), a divergence of 0.8 mrad and pulse duration of 15.6 ns. It was possible to rotate the crystal a maximum of $3.3°$ (internal) from the point of normal incidence ($\phi = 33°$). The largest signal energy is obtained at the point of normal incidence, however, the sum-frequency
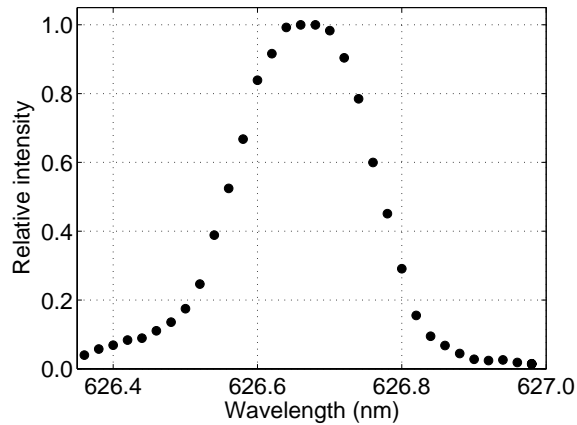
Fig. 5. Spectrum of the sum-frequency beam.
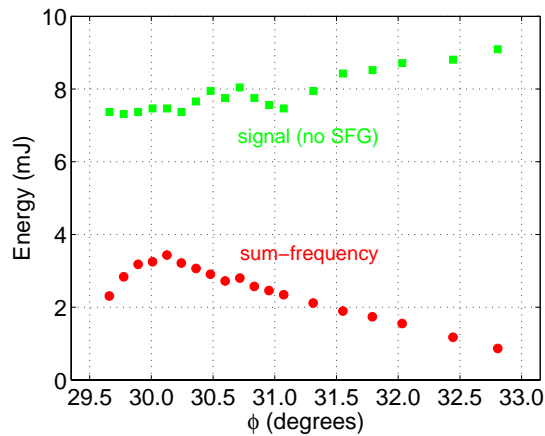
Fig. 6. Signal energy at a polarization rotation angle of 0° (no SFG) and sum-frequency energy at a polarization rotation angle of 28° as functions of the propagation direction in *xy*-plane of KTA ($\theta = 90°$).

energy peaks at the simultaneous phase-matching angle of $\phi = 30.1°$.

Even with a $R = 85\%$ output coupler for the signal where the 1064-nm-to-627-nm energy conversion efficiency is 8.6%, approximately 70% of the *s*-polarized signal component becomes depleted. Consequently, a stronger depletion for the *s*-polarized signal component can be expected for the case when M2 is a high reflector at 1525 nm.

Inherently, it is not possible to angle-tune SF-OPOs when pumped by fixed wavelength lasers, since the simultaneous phase matching condition occurs at a single direction of propagation for a fixed pump wavelength. In our case, Fig. 6 shows that deviating from the simultaneous phase matching angle results in a rapid decrease of sum-frequency energy.

It is difficult to find a single set of Sellmeier coefficients that is accurate throughout the transparency range of a nonlinear crystal and valid for different $\chi^{(2)}$ processes. This is even more so for KTA, for which there are several sets of quite different Sellmeier coefficients reported in the literature [17–19]. We determined which set to use for which process in an *ad hoc* fashion.
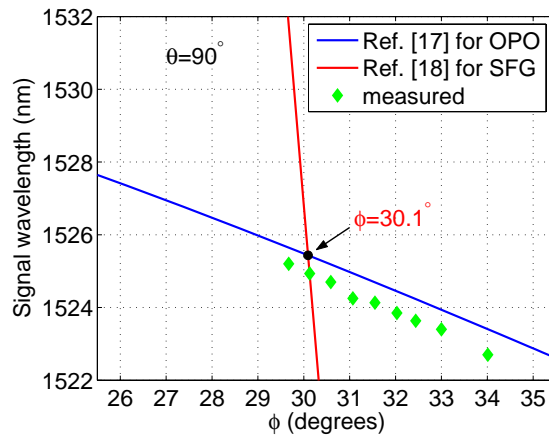
Fig. 7. Tuning curves of the signal wavelength calculated using the refractive index data given in Ref. [17] for parametric generation (signal is *p*-polarized) and refractive index data given in Ref. [18] for SFG (signal is *s*-polarized). Measured signal wavelengths are also shown in the figure.

The simultaneous phase-matching angle determined experimentally is in excellent agreement with the value calculated using the Sellmeier coefficients given in Ref. [17] for parametric generation and those given in Ref. [18] for SFG. Figure 7 shows the tuning curves of the signal wavelength calculated using the refractive index data given in Ref. [17] for parametric generation of the *p*-polarized signal from the *p*-polarized pump and refractive index data given in Ref. [18] for the sum-frequency interaction between the *s*-polarized signal and *p*-polarized pump. The intersection of the two curves occurs at $\phi = 30.1°$, which is the simultaneous phase matching angle for these interactions.

The Sellmeier coefficients given in Ref. [17] are more accurate than those given in Ref. [18] for calculating the wavelengths for parametric generation. Signal wavelengths measured for various values of ϕ are also shown in Fig. 7. They are within ± 0.7 nm of those calculated using the Sellmeier coefficients given in Ref. [17]. However, using the Sellmeier coefficients given in Ref. [18] for parametric generation results in more than 6 nm difference between the calculated (not shown) and measured signal wavelengths.

We also conclude that the Sellmeier coefficients given in Ref. [18] are more accurate than those given in Ref. [17] for calculating the wavelengths of SFG. If the Sellmeier coefficients given in Ref. [17] were used for both parametric generation and SFG, the simultaneous phase matching angle would be calculated to be $\phi = 24°$, which is inconsistent with the experimental result.

4. Conclusion

We have demonstrated a 1064-nm pumped nanosecond SF-OPO that employs a single KTA crystal for both parametric generation and SFG. The output energy at 627 nm is 8.3 mJ, corresponding to an energy conversion efficiency of 21%. Accurate determination of the simultaneous phase-matching angle is essential for achieving a high conversion efficiency for the red output. To our knowledge, this is the first demonstration of a nanosecond SF-OPO. This device provides a simple and efficient method for converting high energy Nd:YAG lasers to a red wavelength.